PNL-10837
UC-606

**A Research Report for
Westinghouse Hanford Company**

# Moisture Measurement for High-Level-Waste Tanks Using Copper Activation Probe in Cone Penetrometer

P. L. Reeder
D. C. Stromswold
R. L. Brodzinski
J. H. Reeves
W. E. Wilson

October 1995

Prepared for
the U. S. Department of Energy
under Contract DE-AC06-76RLO 1830

Pacific Northwest Laboratory
Richland, Washington 99352

## DISCLAIMER

# Executive Summary

Laboratory tests have established the feasibility of using neutron activation of copper as a means for measuring the moisture in Hanford's high-level radioactive waste tanks. The performance of the neutron activation technique to measure moisture is equivalent to the neutron moisture gauges or neutron logs commonly used in commercial well-logging. The principle difference is that the activation of $^{64}Cu$ ($t_{1/2}$ = 12.7 h) replaces the neutron counters used in moisture gauges or neutron logs. For application to highly radioactive waste tanks, the Cu activation technique has the advantage that it is insensitive to very strong gamma radiation fields or high temperatures. In addition, this technique can be deployed through tortuous paths or in confined spaces such as within the bore of a cone penetrometer. However, the results are not available in "real-time".

The copper probe's sensitivity to moisture was measured using simulated tank waste of known moisture content. The copper probe was inserted into the simulated waste by means of a cone penetrometer pipe. A neutron source within the probe provided neutrons that activated the copper after scattering in the waste simulant. Subsequent counting of the gamma rays emitted by the activated copper ($^{64}Cu$) using a low-background spectrometer provided the calibration curve of count rate versus moisture at three moisture contents (15%, 20%, and 25% by weight). These moisture contents were chosen to cover the range of greatest concern for certain Hanford waste tanks.

The calibrations were performed in both "near-field" and "far-field" geometry. The near-field geometry has the neutron source in the center of the Cu probe during the irradiation. The $^{64}Cu$ count rate increases by 3.49 ± 0.09 % for a 1.0 wt. % increase in the moisture content when using this geometry. The time required for a single measurement can be as short as 2 hours for activation and 2 hours for counting when using a neutron source emitting 1.58 x $10^5$ neutrons/s. With these parameters, the uncertainty due to counting statistics is about ±1% which translates into an uncertainty on the moisture content of about ±0.3 wt. %. The far-field geometry has the neutron source at a distance of about 45 cm from the copper probe. In this geometry, the $^{64}Cu$ count rate decreases by 2.80 ± 0.38 % for a 1.0 wt. % increase in the moisture content. Thus the ratio of the near-field to far-field count rates is about twice as sensitive to moisture as the near-field measurement alone. However, to obtain the necessary counting statistics, longer irradiation and counting times are required – or else a stronger neutron source should be used.

The actual wastes in the Hanford tanks contain a measurable neutron flux due to spontaneous fission of actinide nuclides and neutrons from ($\alpha$,n) reactions on light elements. This neutron flux contributes a background to any moisture measurement based on neutron detection. This background was measured by the copper activation technique in Tank TX-118 and was found to be less than 6% of the effective flux measured in the moisture calibration models using a small neutron source.

# Contents

# Figures



# Tables

# 1.0 Introduction

Knowledge of the moisture content of Hanford's high-level radioactive waste tanks is important for many of the tanks. The presence of sufficient moisture in the tank contents (above about 20% by weight) prevents chemical reactions that could release radioactive waste and toxic vapors. Collection of waste samples for moisture analysis is prohibitively expensive due to the high radiation they emit. Moreover, the results may be compromised due to the problems in physical sampling. Consequently alternative methods for in situ measurement of the moisture have been developed. A method used successfully in many of the tanks that have access wells (liquid observation wells) is neutron well logging. In this method, a probe containing a high-energy-neutron source and one or more low-energy-neutron detectors is lowered into the wells. The observed count rate depends mainly on the moisture content of the tank waste because the neutrons interact predominantly with the hydrogen in water to lose their energy. The same neutron-scattering physics applies to the copper activation method of moisture measurement.

Not all Hanford tanks have liquid observation wells to permit access through the tank waste. Cone penetrometers (thick-wall steel pipes with cone-shaped tips) offer the potential of accessing more positions within the tanks without the expense of installing permanent, larger diameter observation wells. The penetrometers have inside diameters of one inch, a size that will not allow access by Hanford's present neutron logging probes.

The present feasibility and calibration tests used hollow copper probes of outside diameter 0.8 inch in order to fit inside penetrometer tubes. These tubes were placed in simulated tank waste of known moisture content. The simulant waste was a mixture of dry chemicals, the main one being $Fe(NO_3)_3 \cdot 9H_2O$. It provided the water, along with iron and nitrogen, for simulating the waste of the ferrocyanide tanks. As part of this project, simulated tank wastes with 15%, 20%, and 25% moisture content were prepared. For the calibration tests, copper probes and a neutron source were inserted into penetrometer tubes in the simulated waste. The neutrons activated the copper after scattering in the waste. Positron decay from the activated copper was counted in a laboratory gamma-ray detection system to obtain the correlation between moisture and the amount of copper activation.

This report describes the preparation of the simulated waste mixtures and the experiments performed to demonstrate the capabilities of the neutron activation technique. These experiments included determination of the calibration curve of count rate versus moisture content using a single copper probe, measurement of the calibration curve based on "near-field" to "far-field" counting ratios using a multiple probe technique, and profiling the activity of the copper probe as a function of the vertical height within a simulated waste barrel.

# 2.0 Neutron Techniques for Moisture Measurements

Neutron techniques have been used for measuring moisture in earth formations for many years (Tittman et al. 1966; Ellis 1990). Some of these same techniques are suitable for measuring the moisture in high-level-waste tanks at Hanford. In these methods a neutron source is lowered into an access well. Energetic neutrons from the source enter the surrounding material and interact mainly with the hydrogen atoms in water. As the neutrons interact with the water, they lose kinetic energy. Some of these lower energy neutrons return to the instrument in the well where they are detected. The neutron detectors are of two types: epithermal or thermal. Thermal neutron detectors count neutrons that have lost essentially all of their energy, whereas epithermal detectors count neutrons that have not quite lost all their energy. Thermal neutron detectors have high efficiency, good statistical accuracy, but high background. Epithermal neutron detectors have poor efficiency, poor statistical accuracy, but low background. The epithermal detectors are much less sensitive to the presence of strong thermal neutron absorbers such as lithium, boron, and gadolinium.

Depending upon the distance between the source location and the point at which the neutrons return to the well, the count rate will either increase or decrease with moisture changes in the material through which the neutrons travel. Specifically, if the neutrons return to a position near the source, the count rate will increase with increasing moisture content. This arrangement is called the "near field" geometry. As the return position within the well moves away from the source location, the change in count rate becomes less sensitive to surrounding moisture until it passes through zero sensitivity and then changes sign for the "far field" geometry. In this arrangement, the count rate decreases with increasing moisture.

Well logging probes used in the oil industry have traditionally used source-to-detector spacings in the far field region in order to penetrate as deeply into the formation as possible. Industries such as civil engineering and agriculture have used moisture gauges with source-to-detector spacings in the near field region to measure moisture in material surrounding air-filled holes. Hearst and Carlson have discussed the differences and applications of these two techniques (Hearst and Carlson 1994).

## 2.1 Commercial Well Logging for Petroleum Industry

The first thoroughly calibrated neutron logging tool was the sidewall neutron porosity (SNP) tool operated by Schlumberger, a major petroleum logging service company (Tittman et al. 1966). Similar tools are still available today for operating in holes of diameter greater than about 12 cm. These tools contain a single epithermal neutron detector ($^3$He tube wrapped with cadmium) and an isotopic neutron source (5 Curies of Am-Be). A spring-loaded, articulated pad on the tool contains the source and detector, holding them against the borehole wall. The pad also provides shielding from unwanted neutrons coming from the borehole rather than from the formation. Because these tools detect epithermal neutrons, they can be used in wells that are filled with air as well as liquid. Furthermore, the epithermal neutron detectors prevent perturbations caused by trace amounts of strong thermal neutron absorbers, such as gadolinium and boron.

The neutron tool that replaced the single-detector epithermal neutron tool in wide usage is the dual-detector, thermal neutron tool. Allen et al. realized that the addition of a second detector would provide compensating effects for the problems inherent in single-detector tools (Allen et al. 1967). By calculating the ratio of counts in two detectors located at different spacings from the neutron source, perturbations caused by mudcake and tool standoff from the wall of the borehole could be greatly reduced. Dual-detector, thermal neutron tools contain two thermal neutron detectors ($^3$He tubes for efficient thermal neutron detection) and a chemical source (16 Curies of Am-Be) (Hearst and Carlson 1994). One detector is located with its center about 38 cm from the source, and the other, larger detector is about 64 cm from the source. The distance of the larger detector from the source promotes deeper sensitivity of the measurement into the formation (15-30 cm for the Hanford vadose

zone). This allows these tools to measure formation properties even when the wells are cased with steel. The longer spacing of the far detector, compared to that of a single detector tool, decreases the tool's ability to measure accurately the moisture of thin beds. There is no shielding to focus the signal on the formation, but a bow spring holds the tool against the borehole wall.

Because these tools detect thermal neutrons, their signal can be affected by trace amounts of elements in the formation that are strong thermal neutron absorbers (Ellis 1990). These elements include the rare earths (e.g., gadolinium) and boron. With the recognition of the disadvantages of using thermal neutron detection has come the increase in popularity of epithermal neutron logging tools (Davis et al. 1981). These tools contain two detectors ($^3$He filled tubes, covered with cadmium to absorb thermal neutrons before they enter the detector) located at different spacings from a neutron source (usually 16 Curies of Am-Be). The detectors are spaced closer to the source than are the comparable detectors in a thermal neutron tool to compensate in part for lower epithermal neutron count rates. The closer spacings make the depth of investigation into the formation slightly shallower, while improving the vertical resolution. Because the measurement is essentially a range of travel of the high energy neutrons as they slow down to epithermal energy, the vertical resolution depends on source-to-detector spacings.

A different type of neutron log has been developed for oil well applications in recent years (Mills et al. 1988; Flanagan et al. 1991). It uses a pulsed source of high-energy neutrons and measures the rate at which epithermal neutrons die away between pulses. The neutrons are generated in the logging tool by a miniature accelerator which uses the D-T (deuterium-tritium) reaction to produce 14-MeV neutrons. Electronic control of the accelerator allows production of pulses of neutrons, as well as elimination of neutrons entirely when the tool is uphole and not energized. This significantly enhances safety for operators and makes transportation of the tool easier. The time-dependent method of measuring moisture is possible because the rate at which high energy neutrons slow down is dependent upon the amount of hydrogen in the formation. The rate at which epithermal neutrons slow down (or die away) is strongly dependent upon moisture content, and it provides a sensitive measure of moisture, especially at low moisture values. This measurement is less affected by the elements that make up the rock matrix (e.g., silicon, oxygen, iron) than are the steady-state source methods such as dual-detector thermal or epithermal logging. The distinction between the two methods is that the steady-state ones essentially measure the distance of travel of the neutrons as they slow down between the source and detector, whereas the time-dependent method measures the time required to slow down. The range is determined mainly while the neutrons still have significant energy. At these higher neutron energies the collisions with the heavier elements in the rock matrix play a significant role in determining the range. In contrast, the slowing down time is determined mainly by collisions when the neutrons have lower energy and are traveling slower. For these lower energies the collisions with hydrogen dominate the neutron slowing down process. Hence sensitivity to hydrogen content is enhanced while the undesirable effects due to non-water components are reduced.

In all these methods, a calibration curve of count rate versus moisture content or die-away time versus moisture content must be generated by laboratory experiments to give quantitative results.

## 2.2 Hanford Waste Tanks

The Hanford waste tanks present difficulties that prevent conventional equipment developed for the petroleum, civil engineering, or agricultural industries from working without modification. The holes into the tanks often have diameters that are too small for conventional petroleum industry equipment. The high radioactivity in the waste tanks creates a gamma-ray background that will overwhelm the neutron counts in conventional neutron detectors. These detectors are typically gas-filled tubes containing $^3$He. Alternative detectors with reduced sensitivity to gamma rays are made of

$BF_3$ or $^{10}B$-lined fission chambers. The neutron logging tools used in the past in the waste tanks have used $BF_3$ detectors. Fission chambers are used in a new probe developed by SAIC for cone penetrometer applications in the tanks. Methods based on neutron counting give results in "real-time"; i.e., the results are available while the probe is in the hole.

The copper activation technique is insensitive to the high gamma-ray background in the Hanford tanks. Only neutrons produce activation of the copper. However, the copper must be removed from the tanks in order to measure its activation. Thus, the results are not available in "real-time" but are delayed by several hours.

# 3.0 Copper Activation Method

In the copper activation method, a source of neutrons provides the means for activation. The source is typically AmBe, PuBe, or $^{252}Cf$, which emit fast neutrons with energies of several MeV. After the neutrons slow down to thermal energy through collisions with surrounding material, they can be absorbed by $^{63}Cu$ (69% abundance of natural copper) to become $^{64}Cu$:

$$^{63}Cu + n \rightarrow {}^{64}Cu$$

The thermal neutron absorption cross section for $^{63}Cu$ is 4.4 b, a relatively large value that helps to provide efficient activation of the copper. The $^{64}Cu$ produced by the activation decays with a half life of 12.7 h. When $^{64}Cu$ decays, three decay paths exist, with the following probabilities:

| | | |
|---|---|---|
| $^{64}Cu \rightarrow {}^{64}Zn + \beta^-$ | 40% | (electron emission) |
| $^{64}Cu + e^- \rightarrow {}^{64}Ni$ | 41% | (electron capture) |
| $^{64}Cu \rightarrow {}^{64}Zn + \beta^+$ | 19% | (positron emission) |

The third decay path (positron emission) leads to a readily detectable signal. The emitted positron annihilates with an electron to give two gamma rays, each with energy 0.511 MeV:

$$\beta^+ + e^- \rightarrow 2\gamma \quad (E_\gamma = 0.511 \text{ MeV})$$

The two gamma rays are emitted simultaneously in opposite directions. Two detectors, located on opposite sides of the source, detect the gamma rays. Requiring the gamma rays to have the proper energy and also be detected in coincidence greatly reduces the background counts. Surrounding the detectors with an anti-coincidence detector and shielding further reduces the background.

Detection of positrons following neutron activation of copper has a distinct advantage in that very few elements produce positrons following thermal neutron capture. In addition, most of the cases where positron emission is possible have much longer half-lives or low branching ratios. The possible interference of positrons from decay of $^{62}Cu$ ($t_{1/2}$ = 9.74 m) produced by (n,2n) reactions is a problem only if the neutron energy is above 12 MeV. The PuBe source used in this work has an average neutron energy of about 4.5 MeV and a maximum energy of about 10.7 MeV. Thus, no interference from other positron activities is expected. Experimentally, no evidence was found in this work for any positron activity other than $^{64}Cu$.

Figure 1 shows a diagram of the neutron activation of copper as it applies to measuring the moisture in Hanford's high-level-waste tanks. A neutron source located inside a hollow copper pipe provides neutrons of high energy. Both the neutron source and the copper are placed inside a steel penetrometer pipe that is surrounded by the tank waste. Fast neutrons from the source readily penetrate the copper and the steel to enter the tank waste. Collisions of the neutrons with hydrogen atoms in the waste provide the dominant means for slowing down the neutrons. The low mass of hydrogen atoms, which is essentially the same as that of the neutron, allows an efficient energy transfer process. After the neutrons have lost their energy, they continue to scatter, gaining and losing some energy in the thermal energy region. Some of these thermal neutrons return to the probe where they are absorbed to activate the copper. The activity of the copper continues to build up from exposure to the neutrons until a state of equilibrium develops between the newly activated copper nuclei and the decay of the previously activated ones. In practice, however, the equilibrium state is not reached because activation is terminated due to time constraints and because sufficient activation exists at shorter times.

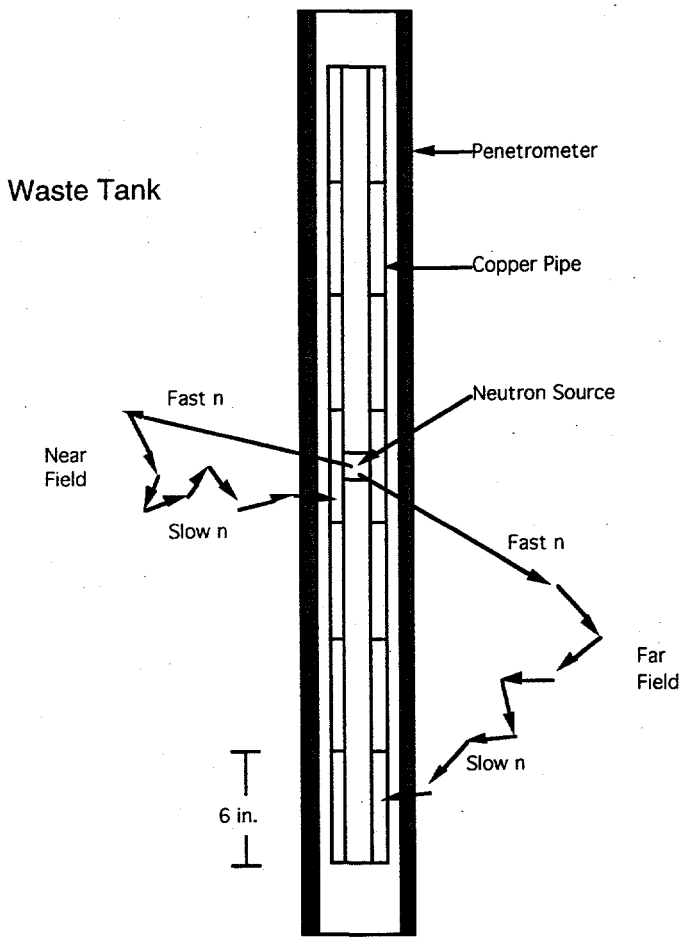


**Figure 1.** Schematic Representation of Cu Probe for Neutron Activation Analysis for Moisture

# 4.0 Equipment

## 4.1 Copper Probe

The copper probe is made of sections of copper pipe that screw together. Each section has a length of 15.2 cm (not including the male threads), outside diameter 2 cm, inside diameter 1.4 cm, and weight about 270 g. Figure 2 shows a drawing of a single copper pipe section. The purity of the copper is ≥99.92%. Each section of copper has an identification number stamped on it. Preparation of the copper probes consisted of simply rinsing the pipes with water and wiping dry to remove surface dirt.

A PuBe neutron source (PNL source M-710) containing 1.2 g of Pu and emitting $1.58 \times 10^5$ n/s was attached to an aluminum source holder which allowed placement inside a copper probe section. The source holder's design positions the source at the center of the copper.

Additional sections of copper pipe can be screwed together above and below the one containing the source. This permits additional moisture measurements when account is taken of the source and detector positions. Both near-field and far-field results can be obtained from one irradiation assuming proper calibrations have been performed.

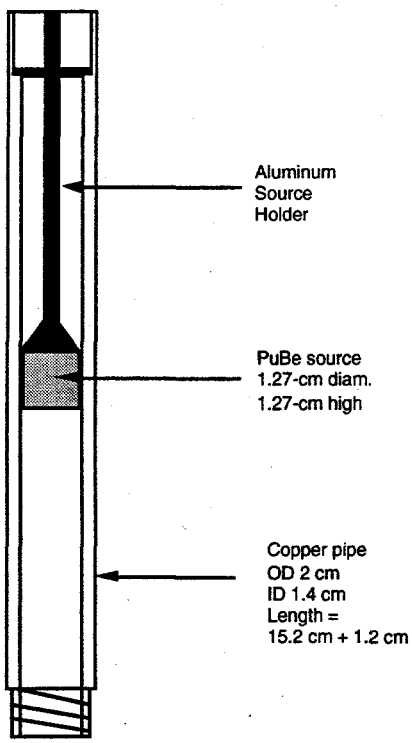


**Figure 2.** Sketch of a Single Cu Probe with Neutron Source and Holder

## 4.2 Calibration Models

The calibration models containing simulated tank waste are made from two 85-gallon drums welded together to increase their height to about 152 cm. The simulant fills the drums to a height of about 140 cm, and the diameter is 68.5 cm. The models have a central cone penetrometer pipe[a] to provide access for the copper probe along the axis of the drums as shown in Figure 3.

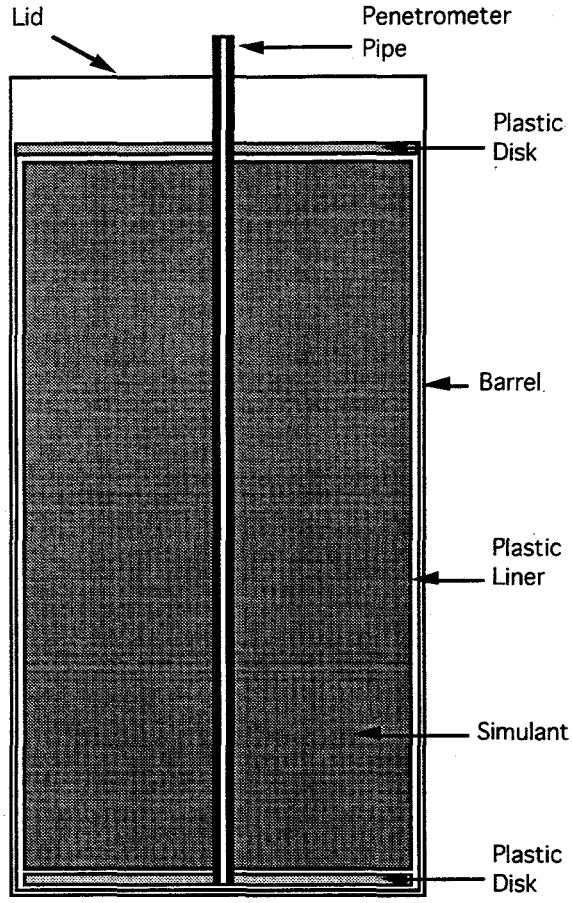


**Figure 3.** Sketch of Moisture Models with Penetrometer Pipe

The penetrometer pipe, a 4130 carbon steel alloy, has an outside diameter of 4.45 cm and an inside diameter of 2.54 cm. A 2.54-cm thick plastic disk with a central hole was placed at the bottom of the barrel to align the pipe on the axis of the barrel. A second 2.54-cm thick plastic disk covered the top of the simulated waste mixture and was sealed with a silicone sealant. Polyethylene bags (0.3-mm thick) were used to line the barrels and the penetrometer pipe to prevent contact of the dry chemicals with steel. This was done to prevent corrosive chemical reactions with the steel. The penetrometer pipes extended about 20 cm above the level of the simulated waste and through a hole in the lid of the barrels.

(a) The penetrometer pipe was obtained from Applied Research Associates, South Royalton, Vermont.

Dry mixtures of chemicals were blended in a cement mixer and used to fill the drums with waste simulants of known moisture contents. The moisture comes from the water of hydration bound in ferric nitrate [$Fe(NO_3)_3 \bullet 9H_2O$] . The chemicals contain elements that are also present in the ferrocyanide waste tanks. The mixing proportions achieve the approximate ratios of the major elements present in the waste and also have similar neutron scattering and absorptive properties. Todd Watson, Westinghouse Hanford Company, calculated the mixing formulas for the models[a]. He used the computer code Monte Carlo Neutron Photon (MCNP) to adjust the chemical proportions so that the neutron spectrum shape simulated an actual spectrum from a Hanford tank. Details of the mixing process and exact compositions for the simulated wastes are given in Appendix A. Samples of each of the three compositions were analyzed by thermal decomposition to determine the actual moisture content.

## 4.3 Counting System

The gamma-ray counting system used to measure the activation of the copper contains two large NaI(Tl) scintillation detectors each having a diameter of 30 cm and a thickness of 20 cm. Each NaI(Tl) detector is surrounded by a plastic anti-coincidence detector (102-cm diameter and 61-cm height) to reduce background. Individual copper pipes were placed on their side between the NaI(Tl) detectors for the most efficient counting geometry. The gap between the NaI(Tl) detectors was about 2.5 cm. Borated paraffin 10-cm thick surrounded the detectors and lead shielding (also 10-cm thick) surrounded the paraffin. The combined shielding and anti-coincidence system resulted in a background of 0.0025 c/s for the 0.511-MeV coincident gamma-ray peaks used to count the $^{64}Cu$.

Coincidence of two 0.511-MeV gamma rays served as the signature for annihilation of the positrons emitted from decay of $^{64}Cu$. Because these gamma rays are emitted in opposite directions, having the copper pipe sandwiched between the two NaI(Tl) detectors provided efficient counting. The electronics used for the data collection are described in more detail in Appendix B. Data were accepted only when there was no simultaneous pulse from the anti-coincidence shield. The coincident pulse height spectra from the two NaI(Tl) crystals were stored in a two dimensional array of 64 channels on each axis. The spectra covered the energy range from approximately 0.1 to 3 MeV. Counting times were typically 120 or 240 minutes. The counts in five channels of the two-dimensional array corresponding to the 0.511-0.511 coincidence peak were summed to give the $^{64}Cu$ count rate.

---

(a) Internal memo from W. T. Watson to D. C. Stromswold dated June 22, 1994, "Calculations of neutronic equivalent simulant composition for 10 st. % moisture U-plant-2 flow sludge."

Internal memo from W. T. Watson to G. T. Dukelow dated June 25, 1993, "Completion of limited calibration of the neutron probe and the associated MCNP model using special simulant filled drums."

Internal memo from W. T. Watson to G. T. Dukelow dated September 24, 1993, "Proof of principle report for in-tank moisture monitoring using an active neutron probe."

Internal memo from C. J. Berglund to H. Toffer dated December 28,1994, "Description of neutron probe moisture calibration assemblies prepared employing a reagent blend."

Internal memo from T. M. Hohl to H. Toffer dated February 16, 1995, "Description of final neutron probe moisture calibration assembly employing a reagent blend."

A data analysis program (MITE2) summed the specified channels, subtracted the detector background, estimated the Compton tails from higher energy gammas, and corrected the count rate back to the time that the copper sample was removed from the calibration model. The details of the data analysis are given in Appendix C. The object of the data analysis was to obtain the count rate per gram of copper equivalent to the initial activity from an irradiation time of infinite length (saturation activity).

## 4.4 Counting Efficiency

The efficiency for counting $^{64}Cu$ was determined from the experiments described in Appendix D. The overall counting efficiency was $4.29 \pm 0.21\%$. Although the geometrical efficiency with the large NaI(Tl) detectors is quite high, the total efficiency is greatly reduced because of the low positron branching fraction (19.3 %) and the fraction of 0.511-MeV gammas which do not appear in the photopeak due to Compton scattering. The primary calibration curve (saturation activity per gram versus moisture content) is not affected by the uncertainty of the counting efficiency. However, this uncertainty is a factor when converting the saturation activity per gram to the effective neutron flux (see below).

# 5.0 Experimental Results

## 5.1 Single Probe Measurements

The primary calibration curve was the saturation $^{64}Cu$ count rate per gram of copper versus the moisture content of the simulated waste model. The calibration curve of effective neutron flux versus moisture content was derived from the primary data by dividing the count rate by the constant factors for counting efficiency, thermal neutron capture cross section, and number of $^{63}Cu$ atoms per gram of copper.

The primary data were obtained from irradiations of a single copper probe (15-cm long) containing the neutron source at the midpoint of the probe. This probe was suspended at the midpoint of the simulated waste model. This configuration represents the near-field irradiation under conditions where there is no additional copper located above or below the single probe. Irradiations were performed for two hours in each of the three models. A second series of irradiations was conducted for times of 14 to 17 hours to obtain improved statistical accuracy. Immediately following each irradiation, the copper probes were transferred to the counting facility where several counts each lasting either 2 or 4 hours were obtained. Weighted average values for the saturation activity per gram from all these irradiations were obtained as described in Appendix C. The statistical uncertainty of the counting data from the 2 hour irradiation and a single 2 hour count was about 1%. The weighted average values from multiple counts of the same sample and from duplicate runs at longer irradiation times gave statistical uncertainties which were about 0.2%.

The results of the single probe calibration runs are summarized in Table 1 and plotted in Figs. 4 and 5. Note that the source position in this and all following tables is relative to the top of the penetrometer pipe. As shown in the figures, the observed count rate/neutron flux increases with increasing moisture content of the waste simulant. This is in agreement with expectations for the near-field geometry. From the slope of the calibration curve, we note that a 1% change in the moisture content causes about a 2 to 4% change in the count rate/neutron flux. Thus the 1% uncertainty in the count rate obtained by a 2 hour irradiation and 2 hour count corresponds to about a 0.50 to 0.25 wt. % uncertainty in the moisture content. These uncertainties can easily be lowered by irradiating the sample for longer times or by counting for longer times. However, there is little to be gained by irradiation times or counting times of more than two half-lives (24 hours).

**Table 1.** Results for Single Probe Moisture Calibration (source at 90.2 cm).[a]

| Moisture (wt. %) | Number of irradiations | Saturation activity per gram (cpm/g) | Effective neutron flux ($n/cm^2 \cdot s$) |
|---|---|---|---|
| 15 | 4 | 2.756 ± 0.004 ± 0.011 | 36.21 ± 0.06 ± 0.15 |
| 20 | 2 | 3.340 ± 0.005 ± 0.014 | 43.88 ± 0.07 ± 0.18 |
| 25 | 2 | 3.644 ± 0.008 ± 0.005 | 47.87 ± 0.10 ± 0.07 |

[a]The first uncertainty gives the statistical uncertainty of the weighted average based on counting statistics alone. The second uncertainty is the standard deviation of replicate measurements. All data have been corrected for gain shift.

Very good statistical accuracy (<1%) was obtained for most of the irradiations. However, in some cases, replicate measurements gave results which differed by 3 or 4%. This problem was identified as being due to gain shifts in the NaI(Tl) counting system. The amplifier gains were calibrated every few days using a source containing $^{137}Cs$ and $^{60}Co$. Generally no adjustment of the gains was required. Apparently, small gain shifts were not caught by this procedure. The activity levels of the $^{64}Cu$ are high enough that peak stabilization electronics would probably solve this problem in the future. From the present data, it was possible to make a gain shift correction based on the ratio of the observed counts to the counts contained in a slightly larger region of interest. The corrected data are presented in Table 1.

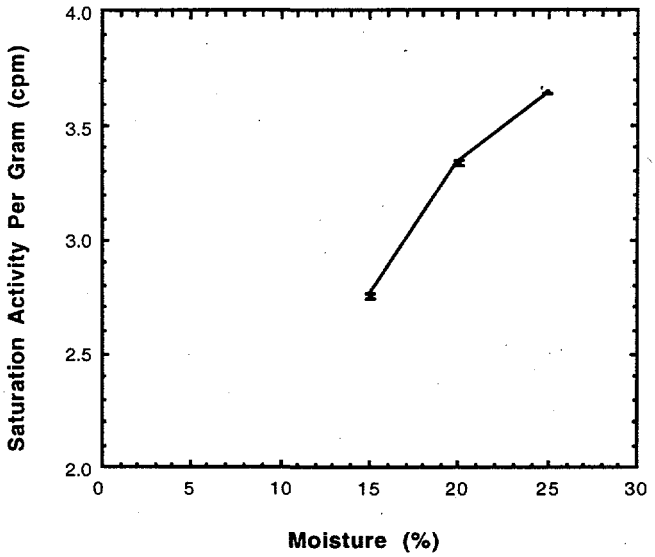


**Figure 4.** Calibration Curve of $^{64}Cu$ Saturation Activity Per Gram Versus Moisture Content for Single Probe Measurements (near-field). Probe is at 0.0 ± 7.6 cm from source. All measurements are at 90.2 cm from top of penetrometer pipe.

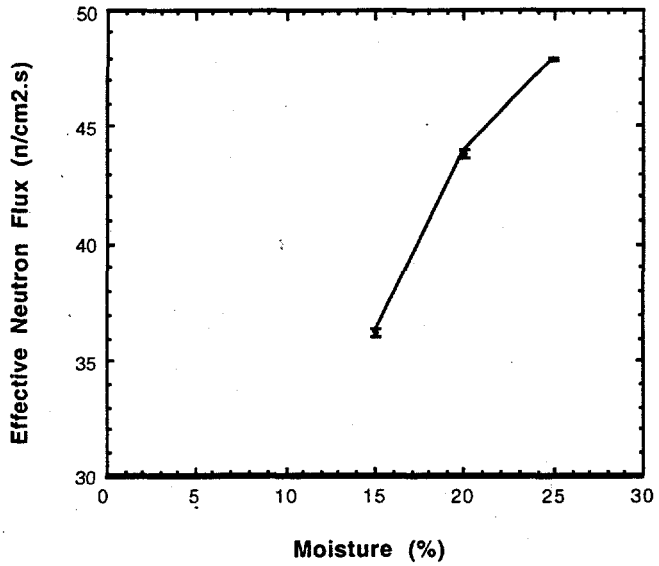


**Figure 5.** Calibration Curve of Effective Neutron Flux Versus Moisture Content for Single Probe Measurements (near-field). Probe is at 0.0 ± 7.6 cm from source. All measurements are at 90.2 cm from top of penetrometer pipe.

## 5.2 Multiple Probe Measurements - Near Field to Far Field Ratio

As described above, additional sensitivity to moisture content can be obtained by measuring the ratio of activity in the near-field geometry to the activity in the far-field geometry. For the Hanford wastes, far field geometry occurs when the detector/probe is placed at 30 cm or more from the neutron source. In this work, multiple copper probes could be screwed together to make a long pipe of whatever length was desired. For practical reasons, we irradiated pipe strings containing five copper probes. The neutron source was placed in the center of the probe next to the top probe. The three lowest probes were at distances of 15.2-, 30.5-, and 45.7-cm from the source. The top probe was attached above the probe containing the source to provide symmetry close to the source, but it was never counted. It was assumed that all results would be symmetric above and below the source provided there were no edge effects due to the finite dimensions of the simulated waste barrels. The string of 4 probes to be counted was centered vertically in the simulated wastes during the irradiations. This meant that the neutron source was 24.1 cm above the position used in the single probe irradiations. As shown by the experiments of the following section, the effective neutron flux as a function of vertical position decreased by about 8.6% at the higher source position but was still on the relatively flat portion of the flux profile.

**Table 2.** Data for Multiple Probe Moisture Calibration (source at 66.0 cm)[a]

| Distance below source (cm) | Moisture (wt. %) | Saturation activity per gram (cpm/g) | Effective neutron flux (n/cm$^2$•s) |
|---|---|---|---|
| 0 | 15 | 2.402 ± 0.021 | 31.56 ± 0.27 |
| 0 | 20 | 2.926 ± 0.013 | 38.45 ± 0.17 |
| 0 | 25 | 3.419 ± 0.016 | 44.92 ± 0.21 |
| 15.2 | 15 | 1.026 ± 0.006 | 13.48 ± 0.08 |
| 15.2 | 20 | 1.176 ± 0.002 | 15.46 ± 0.03 |
| 15.2 | 25 | 1.265 ± 0.009 | 16.62 ± 0.12 |
| 30.5 | 15 | 0.221 ± 0.002 | 2.900 ± 0.028 |
| 30.5 | 20 | 0.198 ± 0.003 | 2.606 ± 0.037 |
| 30.5 | 25 | 0.191 ± 0.003 | 2.510 ± 0.045 |
| 45.7 | 15 | 0.037 ± 0.001 | 0.490 ± 0.014 |
| 45.7 | 20 | 0.031 ± 0.001 | 0.402 ± 0.008 |
| 45.7 | 25 | 0.028 ± 0.001 | 0.370 ± 0.008 |

[a]Uncertainties shown are based only on counting statistics.

For the multiple probe calibrations, the irradiation times were 17 hours or more to achieve good statistical accuracy on the farthest probe. The near-field probe was counted just once for 2 hours, whereas the far-field probes were counted longer as an aid to better statistical accuracy. The results are presented in Table 2 and plotted in Fig. 6.

The near-field count rates increase as the moisture increases and the far-field count rates decrease as the moisture increases just as expected. Thus, the ratio of the near-field rate to the far-field rate is a more sensitive measure of the moisture content than just the near-field rate alone. However, because the effective neutron flux falls off rapidly with distance, it is necessary to irradiate and count for longer time intervals to maintain the required statistical accuracy. Data for the near-field to far-field ratios are presented in Table 3 and Figure 7 for two different far-field distances. Similar data are presented for the fission chamber probe developed by SAIC at a far-field distance of 30.5 cm [a]. The difference between the Cu probe and fission chamber results at 30.5 cm is due to the fact that SAIC used a fission chamber probe for the near detector and a $^{10}$B-lined counter for the far detector. The $^{10}$B-lined counter was thought to have about 9 times the counting efficiency of the fission chamber probe in rough agreement with the ratio of the PNL and SAIC results. The fact that the neutron source is inside the Cu probe in this work but outside the fission chamber in the SAIC work should cause only minor differences in the near/far ratio.

(a) "Phase 1 of Cone Penetrometer Moisture Probe Study," Final report submitted to Westinghouse Hanford Company by Science Applications International Corporation, Task MGJB-SWV-370248-001, March 28, 1995.

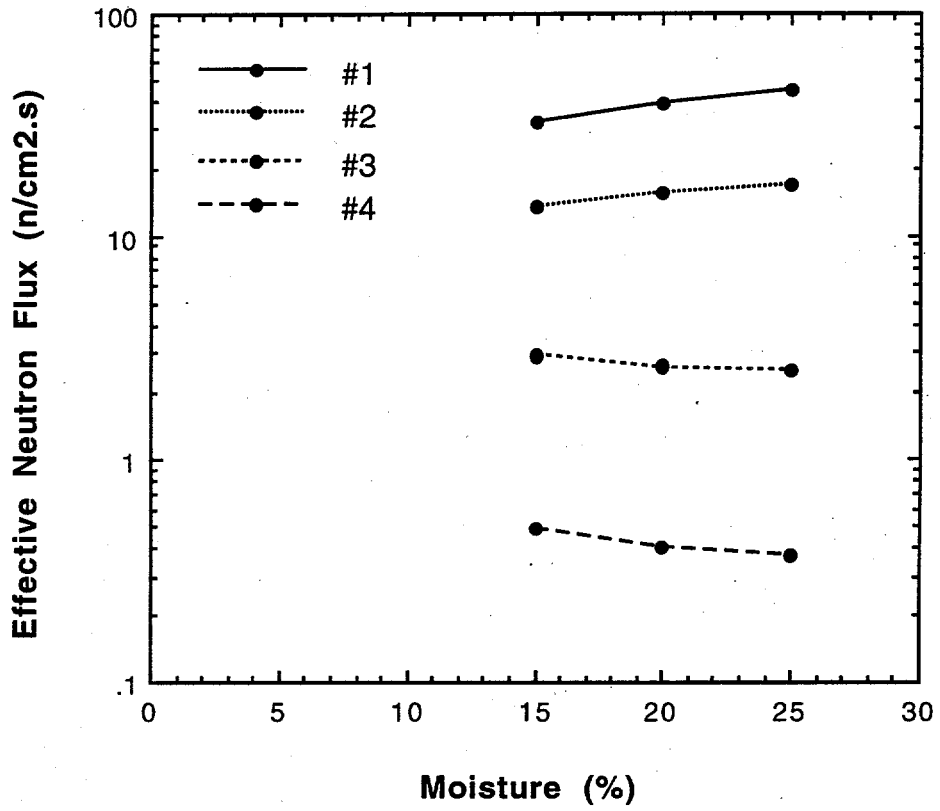


**Figure 6.** Effective Neutron Flux Versus Moisture for Near-Field and Far-Field Probes. Distances of probe from source are: #1 = 0 cm, #2 = 15.2 cm, #3 = 30.5 cm, #4 = 45.7 cm.

**Table 3.** Near-field to far-field count rate ratios at 30.5 cm and 45.7 cm.

| Distance to far-field probe (cm) | Moisture (%) | Near-field / far-field count rate ratio (PNL) | Near-field / far-field count rate ratio (SAIC) |
|---|---|---|---|
| 30.5 | 15 | 10.9 ± 0.3 | 1.4 |
| 30.5 | 20 | 14.8 ± 0.2 | 2.0 |
| 30.5 | 25 | 17.9 ± 0.3 | 2.6 |
| 45.7 | 15 | 64 ± 2 | - |
| 45.7 | 20 | 96 ± 2 | - |
| 45.7 | 25 | 122 ± 3 | - |

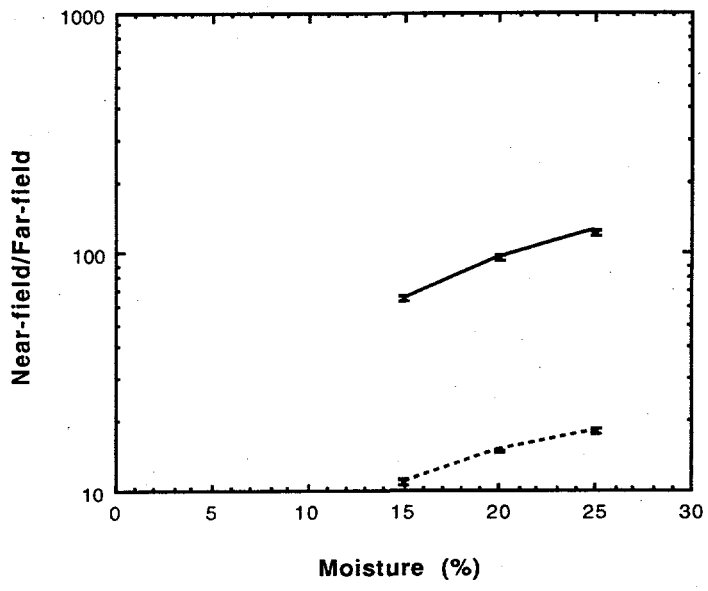


**Figure 7.** Ratio of Near-Field to Far-Field Count Rates. Solid curve is position #1 (0.0 cm) to position #4 (45.7 cm) ratio. Dashed curve is position #1 (0.0 cm) to position #3 (30.5 cm) ratio.

As shown in Table 4, a convenient way to assess the relative sensitivities of the various configurations is to look at the slope of the count rate or count rate ratio versus moisture calibration curves. All slopes were calculated based on the difference of the 15% and 25% data points divided by the average of the 15% and 25% data points. The estimated slope of the count rate ratio of the SAIC fission chamber data is also included. The slight discrepancy with the PNL slope may be due to the slightly different lengths of the copper probe (15.2 cm) and the fission chambers (11.4 cm). Note that the slope of the near-field to far-field ratio (45.7 cm) is about twice as sensitive as the near-field (0.0 cm) count rate alone. However, the fractional uncertainty on the slope of the near-field to far-field count rates is greater than the fractional uncertainty of the near-field slope even though extra irradiation and counting times were used to increase the statistical accuracy of the far-field data. Thus, the extra effort required to obtain the near-field to far-field ratio does not seem worthwhile, especially since the near-field data has adequate sensitivity for the problem of interest.

**Table 4.** Slope of Moisture Calibration Curves for Various Configurations

| Configuration | Slope = % change in count rate for a 1 wt. % increase in moisture content |
|---|---|
| Count rate 0.0 cm from source | +3.49 ± 0.09 |
| Count rate 15.2 cm from source | +2.09 ± 0.10 |
| Count rate 30.5 cm from source | -1.44 ± 0.20 |
| Count rate 45.7 cm from source | -2.80 ± 0.38 |
| Count rate ratio, 0.0 / 30.5 (PNL) | +4.9 ± 0.3 |
| Count rate ratio, 0.0 / 30.5 (SAIC) | +3.4 |
| Count rate ratio, 0.0 / 45.7 | +6.1 ± 0.4 |

From the data in Tables 1 and 2, we note that the near-field count rate obtained with the source at 66.0 cm in the multiple probe configuration is significantly lower than the count rate obtained with the single probe at 90.2 cm. This is true for all three moisture models, but the 25% model has the smallest fractional decrease. There are two possible explanations for this discrepancy. One possibility is that the presence of additional copper probes above and below the probe with the neutron source causes the effective neutron flux to be lowered due to absorption of neutrons. This possibility was checked at both the 66.0- and 90.2-cm positions for irradiations in the 15% moisture model. The single probe count rates at both the 66.0- and 90.2-cm positions were identical within the statistical accuracy to the multiple probe count rates at the corresponding positions Thus, the presence of the extra copper does not significantly affect the neutron flux at the probe with the source. An alternative explanation is that the absorption and scattering of neutrons is different at the two locations so that the effective neutron flux is actually lower at the 66.0 cm position. The 25% moisture model should be the least affected by edge and end effects which is consistent with the trend of this discrepancy. The flux profile was explored by performing the vertical scan described in the next section.

### 5.3 Vertical Position Scan

In principle, the simulated waste models were sufficiently tall that a constant count rate should be obtained over an extended region in the middle of the barrels. The count rate should decrease near the top and bottom of the barrels due to loss of neutrons from the outer surfaces. To verify this expectation, irradiations of a single probe were done as a function of the vertical height. Irradiation times and counting times were chosen to give statistical uncertainties of less than 1%. All measurements were done in the 15% moisture model as this composition was expected to have the largest effects due to neutron loss at the outer surfaces. The results are shown in Table 5 and plotted in Fig. 8. A special irradiation was conducted with the neutron source inside a single copper probe but suspended in air as far as possible from materials which could thermalize the neutrons and backscatter into the probe. The activity produced in this irradiation represents the amount of $^{64}Cu$ produced by fast neutrons and by neutrons thermalized within the copper. This represents a background relative to the neutrons which thermalize in the simulant and then activate the copper. This background (shown as the last entry in Table 5) was subtracted from every data point to obtain the corrected curve shown in Fig. 8. Note that vertical profiles of the higher moisture models would be expected to have longer and flatter profiles in the middle of the model compared to the profile shown for the 15% moisture model.

From the multiple probe results for the 15% moisture model given in Table 3, we know that the neutron flux is reduced by a factor of about 64 at a distance of 45 cm from the source. Thus the neutron flux should not be perturbed by end effects until the probe is within about 45 cm of the top of the simulated waste. The 66.0 cm position corresponds to 45.7 cm from the top of the simulant.

Thus the reduction of 5 - 10% in count rate at the 66.0 cm position is several times the expected loss of neutron flux of 1 - 2%. The cause of this discrepancy is unknown at this time.

The radial distance from the source to the wall of the model is 34 cm which means that effects of several % might be expected relative to a tank with an infinite radial distance. However, the radial effects in the simulant models should be constant as a function of vertical height unless inhomogeneities in the simulant are significant.

The calibration models are clearly not so large as the actual waste tanks at Hanford. Computer modeling could determine the effects on the calibration that would result from scaling the volume up to that which effectively appears "infinite" to the neutrons from the source. All of the wall and end effects could be determined by use of Monte Carlo neutron transport codes to simulate the dimensions of the models or actual wastes with infinite dimensions. Such calculations were planned as part of this work, but had to be omitted due to lack of funds.

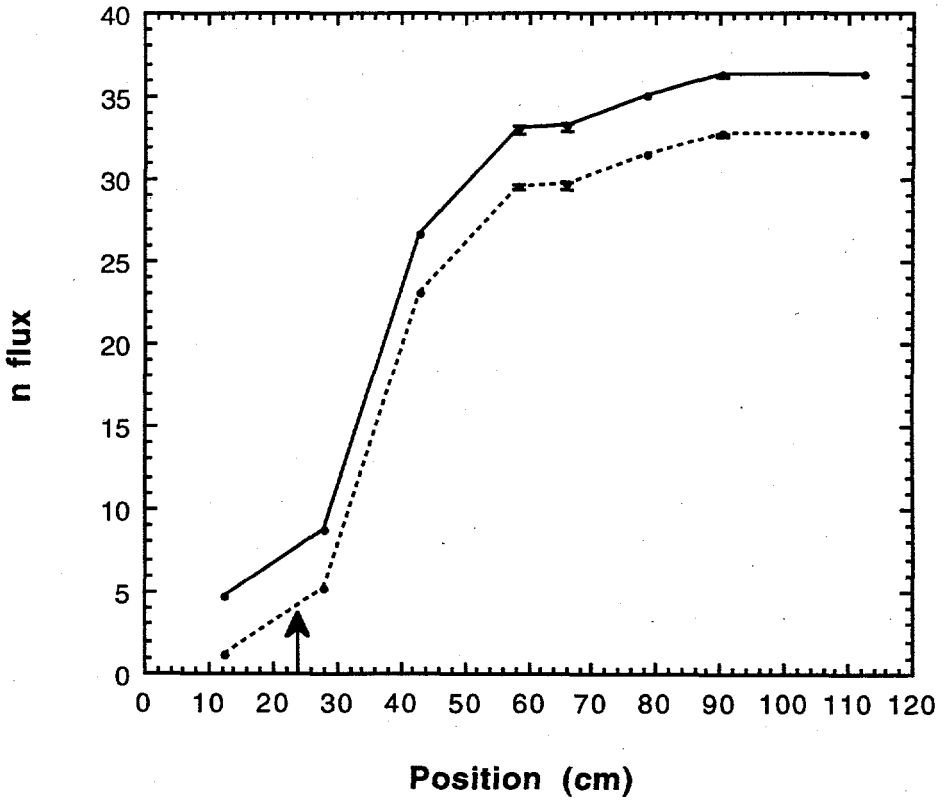


**Figure 8.** Vertical Profile of Effective Neutron Flux in 15% Moisture Model. Solid line = measured values. Dashed line = measured values minus contribution from direct neutron activation of copper. Distances are measured from top of penetrometer pipe. Arrow indicates position of top of simulated waste.

**Table 5.** Results of Vertical Scan in 15% Moisture Model

| | Source Position (cm) | Saturation Activity/g (cpm) | Sigma | Standard Deviation | N flux $n/cm^2 \cdot s$ | Sigma | Standard Deviation |
|---|---|---|---|---|---|---|---|
| | 112.4 | 2.760 | 0.007 | | 36.26 | 0.09 | |
| | 90.2 | 2.745 | 0.020 | | 36.07 | 0.26 | |
| | 90.2 | 2.771 | 0.012 | | 36.41 | 0.15 | |
| | 90.2 | 2.752 | 0.007 | | 36.16 | 0.09 | |
| | 91.4 | 2.757 | 0.007 | | 36.22 | 0.09 | |
| | 90.2[a] | 2.760 | 0.009 | | 36.26 | 0.12 | |
| Wt. Ave. = | 90.2 | 2.757 | 0.004 | 0.010 | 36.22 | 0.05 | 0.13 |
| | 78.7 | 2.662 | 0.008 | | 34.98 | 0.10 | |
| | 66.0 | 2.504 | 0.007 | | 32.89 | 0.09 | |
| | 66.0 | 2.542 | 0.007 | | 33.40 | 0.09 | |
| | 66.0[b] | 2.525 | 0.022 | | 33.17 | 0.29 | |
| Wt. Ave. = | 66.0 | 2.523 | 0.005 | 0.019 | 33.15 | 0.06 | 0.26 |
| | 58.4 | 2.523 | 0.007 | | 33.15 | 0.09 | |
| | 58.4 | 2.502 | 0.007 | | 32.87 | 0.09 | |
| Wt. Ave. = | 58.4 | 2.513 | 0.005 | 0.015 | 33.02 | 0.07 | 0.19 |
| | 43.2 | 2.029 | 0.006 | | 26.66 | 0.08 | |
| | 27.9 | 0.660 | 0.003 | | 8.68 | 0.04 | |
| | 12.7 | 0.360 | 0.002 | | 4.73 | 0.03 | |
| | 0.0[c] | 0.269 | 0.002 | | 3.54 | 0.03 | |

[a]Irradiation with 3 probes.
[b]Irradiation with 5 probes.
[c]This irradiation was performed in air without nearby moderators.

## 5.4 Neutron Flux from Actinide Wastes

The actual wastes in the Hanford tanks contain a measurable neutron flux due to spontaneous fission of certain actinide nuclides. In addition, alpha decay of actinide nuclides can produce neutrons from ($\alpha$,n) reactions on light elements such as carbon, nitrogen, and oxygen in the wastes. This neutron flux will contribute a background to any moisture measurement based on neutron detection. In actual practice, this background should be measured in order to make the necessary correction to the observed effective neutron flux. In the case of the neutron activation of copper technique, the background flux is measured simply by irradiating a copper probe without using the neutron source.

As an example, an experiment to measure the background neutron flux in Tank TX-118 was carried out in Aug. of 1994. Four copper probes were placed at different locations in the tank and irradiated for about 72 hours. These probes were counted beginning about 30 hours after the end of the irradiation. The probes used in this experiment were larger diameter than the probes normally used and contained about 38% more copper. The counting efficiency was not measured for this size probe, but it is not expected to vary much from the efficiency of the smaller probes. However, the probes were irradiated in liquid observation wells (LOWs) which have some boron in the fiberglass used in the LOWs. Thus there is an unknown correction because of the flux depression caused by the LOWs. The measured effective neutron fluxes are shown in Table 6.

**Table 6.** Effective Neutron Flux in Tank TX-118[a]

| Sample I.D. | Effective neutron flux ($n/cm^2 \cdot s$) |
|---|---|
| AA008 | 0.741 ± 0.016 |
| BB002 | 2.043 ± 0.082 |
| BB003 | 2.120 ± 0.081 |
| BB004 | 2.163 ± 0.079 |

[a]Uncertainties shown are based only on counting statistics.

The fluxes in Table 6 have unknown systematic errors due to the counting efficiency and the LOWs, but they represent the level of neutron background to be expected under actual measurement conditions. The relative values measured here are consistent with measurements performed with a neutron counter system at the same locations. When compared with the effective fluxes given in Table 1, note that the background flux might be as much as 6% of the flux observed using the particular source in this work. Although this background can be corrected via a separate measurement, one could also use a stronger source to minimize the effect of the background contribution.

The neutron activation of copper technique could be used as an indication of the actinide content of a waste tank. However, because the neutrons come from both spontaneous fission and ($\alpha$,n) reactions, defining the calibration curve is more complicated. For example, the spontaneous fission rate is dependent on the isotopic composition of the Pu component. Likewise, the ($\alpha$,n) rate is dependent on the light element composition. If these compositions are known, the neutron flux measured by the copper probe technique could be used to measure the actinide content and distribution in the tank.

# 6. Conclusions

Laboratory experiments using simulated Hanford tank wastes have shown that the neutron activation of copper method will accurately measure moisture in the 10 to 25 wt. % range. The time required for a single measurement can be as short as 2 hours for activation and 2 hours for counting when using a neutron source emitting $1.58 \times 10^5$ neutrons/s. Using a single copper probe, the slope of the calibration curve of saturation activity per gram versus moisture was found to be $+3.49 \pm 0.09$ which means that a 1 wt. % increase in the moisture content causes a 3.5% increase in the saturation activity. Statistical uncertainties in the counting data of ±1% can easily be obtained. Thus, the relative moisture content can be determined to less than 0.3 wt. %.

The absolute moisture content depends on how well the simulated waste models prepared in this work conform to the actual Hanford wastes. There is a further systematic uncertainty in the calibration curve because the models had finite dimensions relative to the range of the neutrons whereas the actual Hanford waste tanks represent infinite dimensions. This uncertainty could be eliminated by performing Monte Carlo neutron transport calculations to duplicate the observed results and then using the parameters obtained from these fits to model wastes with infinite dimensions.

For application to highly radioactive waste tanks, the Cu activation technique has the distinct advantage that it is insensitive to very strong gamma and beta radiation fields. Another virtue of this technique is its simplicity - only a copper pipe and a neutron source need to go into the cone penetrometer pipes of the waste tanks. Although the results of the activation technique are not available while the probe is in the waste tanks, the results can be available within a few hours of the removal of the probe.

The calibrations were performed in both "near-field" and "far-field" geometry. It was demonstrated that the $^{64}Cu$ count rate increases with increasing moisture when using the near-field geometry and decreases with increasing moisture in the far-field geometry. The ratio of the near-field to far-field count rates is about twice as sensitive to moisture as the near-field measurement alone. However, to obtain the necessary counting statistics, longer irradiation and counting times are required – or else a stronger neutron source should be used. The extra effort to obtain near-field to far-field ratios is probably not cost-effective because acceptable sensitivity to moisture content is easily obtained with the near-field measurements alone.

Boron is a strong absorber of neutrons, and its presence could distort the calibration curves determined here. Use of the cone penetrometer eliminates concerns about the boron content of the tubes of the liquid observation wells. No attempt was made in this work to investigate the effect of small amounts of boron in the waste itself. However, Monte Carlo computer models could reliably predict its effects.

Only the vertical profile of the effective neutron flux in the 15% moisture model was measured here. It is desirable to do scans of the other moisture models to see whether the predicted profiles are obtained.

# Acknowledgments

Todd Watson, Westinghouse Hanford Company (WHC), determined the chemical mixing formulas for the waste tank simulants. Ted Hohl and his associates from WHC helped with construction of the calibration models in mixing and packing the materials used as waste simulants. Analysis of the moisture content of the simulated waste was performed by Scott Barney of WHC. Pacific Northwest Laboratory is operated for the U.S.Department of Energy by Battelle Memorial Institute under Contract DE-AC06-76RLO 1830.

# References


Alger, R. P., S. Locke, W. A. Nagel, and H. Sherman. 1972. "The dual-spacing neutron log-CNL," *J. Pet. Tech.* 24, 1073-1083.

Allen, L. S., C. W.Tittle, W. R. Mills, and R. L Caldwell. 1967. "Dual-spaced neutron logging for porosity." *Geophysics*, 32, 60-68.

Davis, R. R., J. E. Hall, Y. L. Boutemy, C. Flaum, and H. Sherman. 1981. "A dual prososity CNL logging system," *Soc. Pet. Eng.* 56th Ann. Fall Mtg., SPE 10296.

Ellis, D. V. 1987. *Well Logging for Earth Scientists*, Elsevier, New York.

Ellis, D. V. 1990. "Some insights on neutron measurements." *IEEE Trans. Nucl. Sci.* 37(2), 959-965.

Flanagan, W. D., R. L. Bramblett, J. E. Galford, R. C. Hertzog, R. E.Plasek, and J. R.Olesen. 1991. "A new generation nuclear logging system." *SPWLA 32nd Annu. Logging Symp. Trans.* (Soc. Prof. Well Log Analysts, Houston) paper Y.

Hearst, J. R, and R. C. Carlson. 1994. "A comparison of the moisture gauge and the neutron log in air-filled holes." *Nuclear Geophysics*, 8, 165-172.

Mills, W. R., L. S. Allen, and D. C.Stromswold. 1988. "Pulsed neutron porosity logging based on epithermal neutron die-away." *Nucl. Geophysics*, 2 (2), 81-93.

Tittman, J., H.Sherman, W. A. Nagel, and R. P. Alger. 1966. "The sidewall epithermal neutron porosity tool." *J. Pet. Technol.* 18, 1351-1362.

# Appendix A

## Preparation of Simulated Wastes

# Appendix A

## Preparation of Simulated Wastes

The simulated Hanford tank wastes were designed to have a composition with neutron transport properties similar to those expected for U-Plant-2 flowsheet sludge found in many ferrocyanide watch-list tanks. The flowsheet sludge was estimated to originally have had a moisture content of 66%. A Monte Carlo radiation transport code (MCNP, Ver. 4A) was used to model the geometry, materials, and transport of neutrons through the simulated waste. The moisture content was determined by the amount of hydrated ferric nitrate in the mixture. Other components were adjusted until the neutron spectrum at the probe location matched the spectrum calculated for the U-Plant-2 sludge. The resultant compositions gave mixtures with the same neutron scattering and absorption characteristics as the tank waste, but with the specified moisture content. Table A.1 shows the chemicals used in making the models.

**Table A.1.** Reagent Blends for Tank Simulant Models and Filling Height

| Compound | Formula | 25% Moisture Wt. (kg) | 20% Moisture Wt. (kg) | 15% Moisture Wt. (kg) | 10% Moisture[a] Wt. (kg) |
|---|---|---|---|---|---|
| Ferric nitrate | $Fe(NO_{3)3}•9H_2O$ | 425.1 | 348.8 | 261.6 | 174.8 |
| Sodium Nitrate | $Na_2NO_3$ | 200.2 | 272.8 | 327.6 | 386.8 |
| Sodium Sulfate | $Na_2SO_4$ | 37.7 | 39.5 | 60.0 | 65.7 |
| Ferric oxide | $Fe_2O_3$ | -- | 15.1 | 36.4 | 47.7 |
| Aluminum oxide | $Al_2O_3$ | 7.7 | 10.6 | 1.4 | 1.7 |
| Sodium chloride | NaCl | 1.4 | 1.8 | 0.7 | -- |
| Graphite | C | 10.4 | 11.4 | 12.1 | 23.3 |
| Total Weight (kg) | | 682.5 | 700.0 | 699.8 | 700.0 |
| Total Weight (lb) | | 1504.7 | 1543.2 | 1542.8 | 1543.2 |
| Distance from top of penetrometer pipe to top of stimulant (cm) | | 17.5 | 18.7 | 23.8 | -- |

[a]The 10% moisture simulant was not constructed.

The chemicals were mixed in 35 kg batches to build the models up in layers. For each batch the chemicals were added to a cement mixer to mix them thoroughly. They were then transferred to the

barrels into which cone penetrometer pipes were already placed. The penetrometer pipes were centered in the bottom of the barrel by a 1.9-cm thick plastic disk having a diameter comparable to the diameter of the barrel and a central hole to accommodate the pipe. A similar disk was placed at the top of the simulated waste and was sealed with silicone caulking. Each layer of chemical was tamped with a steel rod to increase the packing density of the mixture so that it more closely matched that of the Hanford models. About 20 batches were required to fill the barrels. Note that although calculations were performed to determine the composition of a 10% moisture model, this model was not constructed due to lack of funds. Westinghouse Hanford Company constructed the models for the Pacific Northwest Laboratory. Table A.2 shows the moisture content and the density of the three models. The moisture is specified in the table as the "design" moisture, based on the chemical formulas and weighed mass of chemicals, and "sample" moisture, based on laboratory analysis of the collected samples. The density was calculated from the weight of the chemicals added to the barrel and from the volume filled. The volumes were calculated based on the height of the simulant after the mixtures had been allowed to settle for about 2 weeks.

**Table A.2** Moisture and Density of Calibration Models

| Design Moisture (% by weight) | Sample Moisture (% by weight) | Density ($g/cm^3$) |
|---|---|---|
| 15 | 14.82 ± 0.60 | 1.411 |
| 20 | 19.39 ± 0.35 | 1.360 |
| 25 | 17.59 ± 0.46 | 1.314 |

The results shown for the Sample Moisture are based on the average of two measurements and the uncertainty listed is the difference of the two values from the average. The measurement is based on the weight loss from thermal decomposition of the $Fe(NO_3)_3 \cdot 9H_2O$. Note that the 15% and 20% models have excellent agreement between the design moisture and the sample moisture. However, the sample moisture for the 25% model is very different from the design moisture. This discrepancy is understood as follows.

The chemicals were mixed in 20 batches of 35 kg each, as described above. However, the bottom two batches and top two batches on all the models used some older ferric nitrate instead of the newer ferric nitrate purchased specifically for this project. It was felt that use of the older ferric nitrate at the top and bottom would not perturb the composition in the center where the measurements were to be made even if the older ferric nitrate had lost some of its water. The samples to be analyzed for moisture content from the 15% and 20% models were drawn from the middle batches where the new ferric nitrate was used. However, due to an oversight, the sample from the 25% model had to be drawn from one of the top batches which used the older ferric nitrate. It is quite apparent that the older ferric nitrate had indeed lost a significant portion of its water. Thus the sample analyzed for the 25% model is not a representative sample for the middle of the barrel where the measurements were made. Because of the good agreement of the other two models between the design moisture and sample moisture, we have adopted the design moisture for all three models for use in plotting the calibration curves.

The models were placed on pallets consisting of a 1.9-cm thick plywood sheet supported on 10.2-cm high wooden studs. Neutron scattering from the concrete laboratory floor might have a small effect on the neutron flux near the bottom of the model, but this effect was not measured. Nearly all the measurements reported here were performed at the midpoint of the simulant or above.

# Appendix B

# Electronics for Counting $^{64}Cu$

# Appendix B

## Electronics for Counting $^{64}Cu$

The electronic diagram for the NaI(Tl) coincidence spectrometer is shown in Fig. B1. The entire top part of the NaI(Tl) and plastic scintillators are raised and lowered by an electric motor to allow insertion of the samples to be counted. The coincidence time window is about 200 ns.

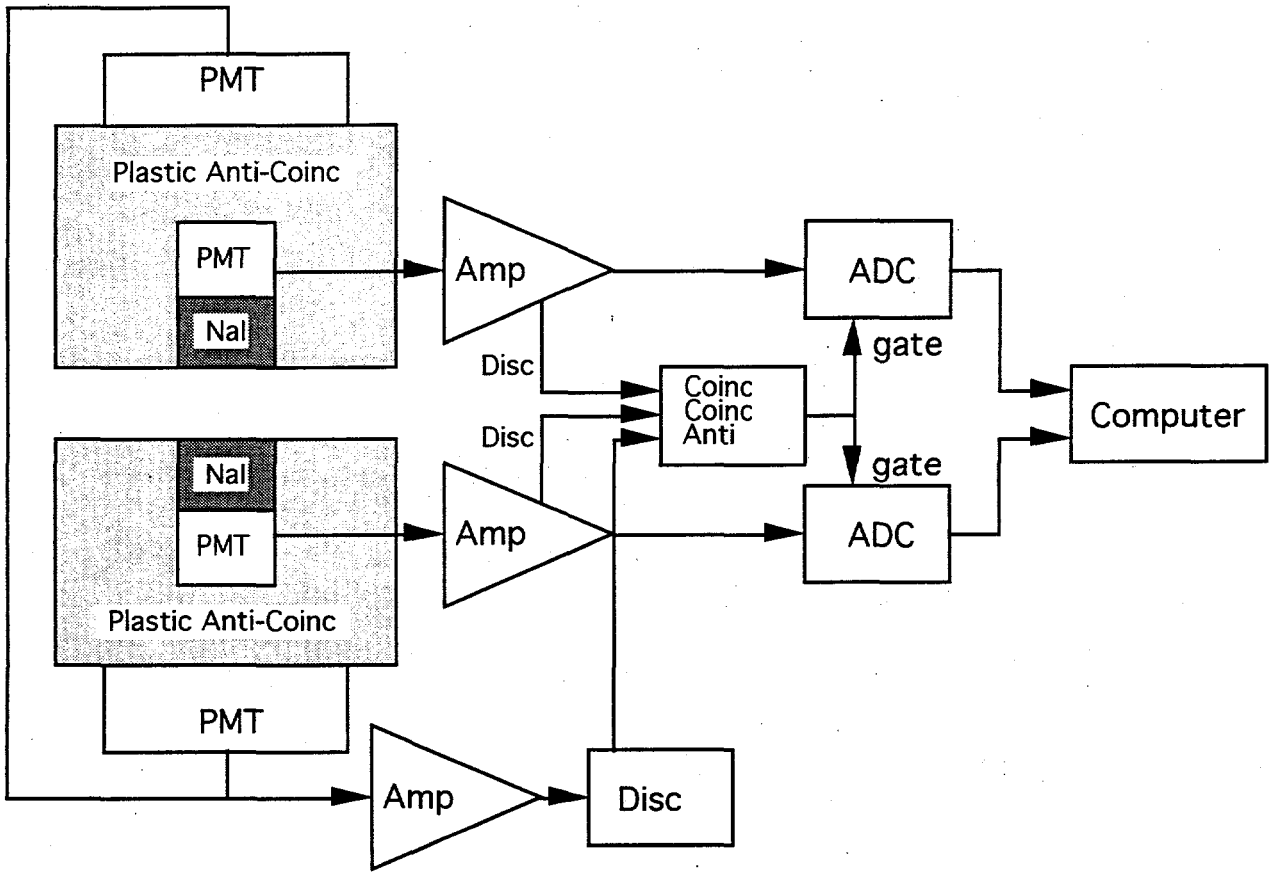


**Figure B.1.** Electronic Diagram for NaI(Tl) Coincidence Spectrometer

The calibration source was a mixture of $^{137}Cs$ and $^{60}Co$. Calibration of the amplifier gains of the NaI(Tl) detectors was performed by a program called DPB. The pulse height spectrum of each NaI(Tl) detector was stored in a separate 256 channel spectrum. The amplifier gains were adjusted to place the 0.662-MeV peak of $^{137}Cs$ in channel 57-58 and the sum peak at 2.5057 MeV from $^{60}Co$ in channel 204.

Because of memory restrictions, the two parameter data acquisition program condensed the 256 channel spectra to 64 channels on each axis. Channel 0 on the Y-axis stored all the counts in the X detector which were not in coincidence with the Y detector. Likewise, channel 0 on the X-axis stored non-coincident counts in the Y detector. Fig. B.2 shows an example of the non-coincident spectrum in the X detector from a $^{64}Cu$ sample. The most prominent peak is due to 0.511-MeV events from

$^{64}$Cu which did not happen to give any pulse in the other detector. The figure also shows the same data when gated by coincidence events in the Y detector corresponding to the three channels containing the 0.511-MeV peak. Note that nearly all the higher energy events are eliminated by the coincidence gate requirement. When the same gate requirement (channels 10, 11, and 12) is applied on both detectors, the interfering counts become negligible.

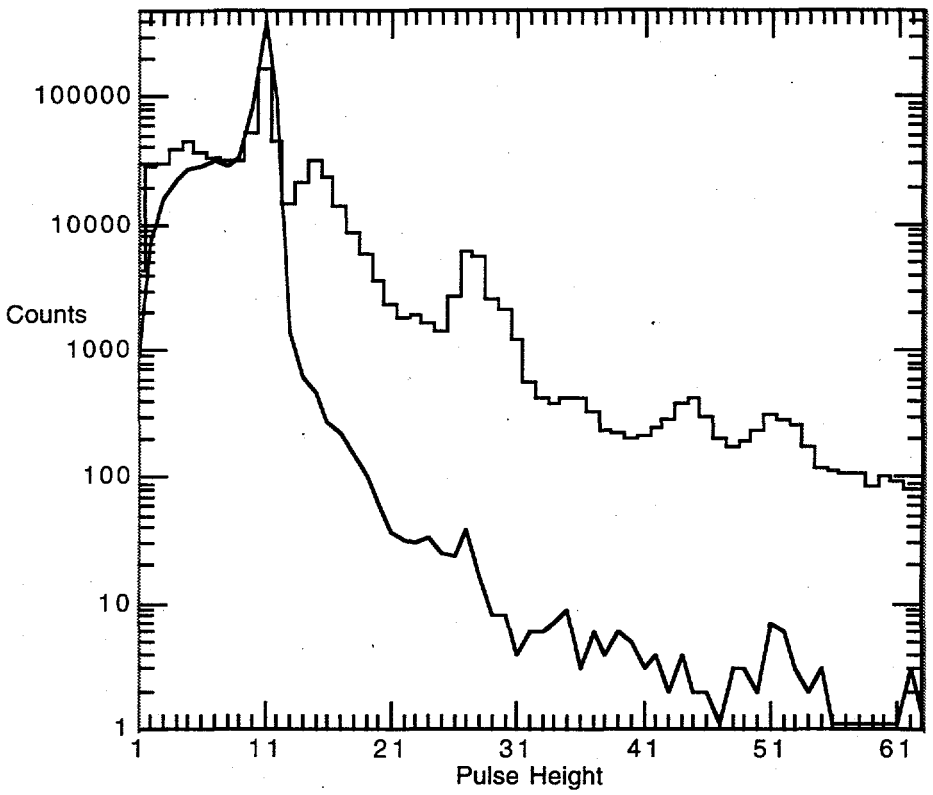


**Figure B.2.** Histogram Curve Is The Pulse Height Spectrum in the X Detector When There Is No Coincident Pulse in the Y Detector. Smooth curve is the pulse height spectrum in the X detector when gated by channels 10, 11, and 12 in the Y detector.

Figure B.3 shows the two-parameter contour display of coincident events for a $^{64}Cu$ sample. The number of counts is proportional to the intensity of the gray scale (fully black corresponds to more than 20,000 counts). The 0.511-MeV events from decay of $^{64}Cu$ appear as the large mountain at channel (11, 11) in the XY plane. The ridges corresponding to Compton scattering events are not included in the region defined as the $^{64}Cu$ peak. Only the counts in channels (10,11), (11,11), (12,11), (11,10), and (11,12) were summed to give the $^{64}Cu$ counting rate. For this set of data, the $^{64}Cu$ counting rate was 4,236 ± 6 cpm.

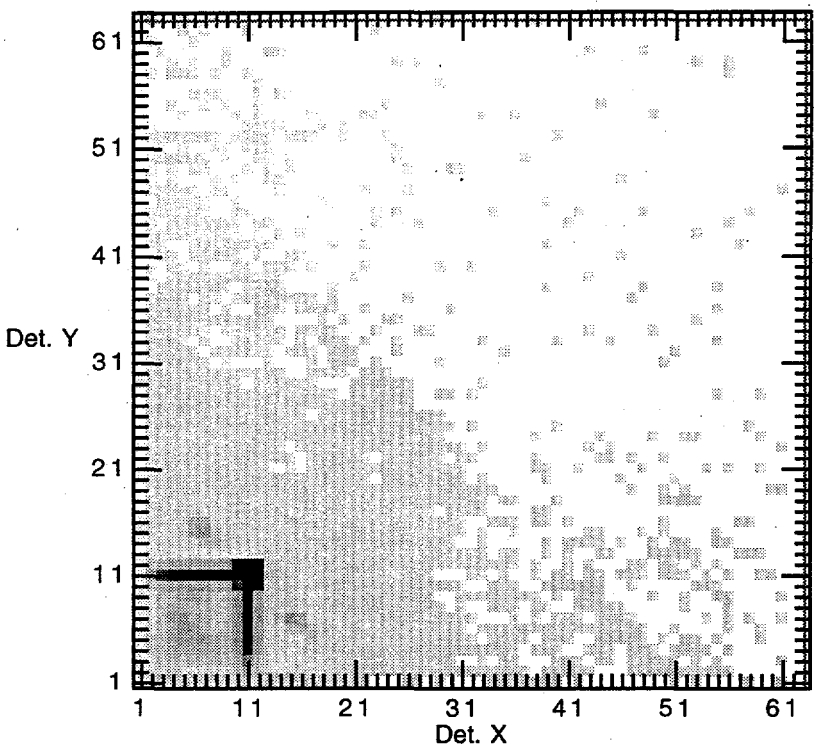


**Figure B.3.** Two-Dimensional Contour Display of $^{64}Cu$ Coincident Events. Full Scale (Black) = >20,000 Counts.

A background count was obtained by placing a copper probe which had never been irradiated in the sample position and counting for about 55 hours. The two-parameter data for this background count are shown in Fig. B.4. The gray scale is set so that fully black corresponds to more than 200 counts. The region of interest for $^{64}Cu$ has 0.166 ± 0.007 cpm.

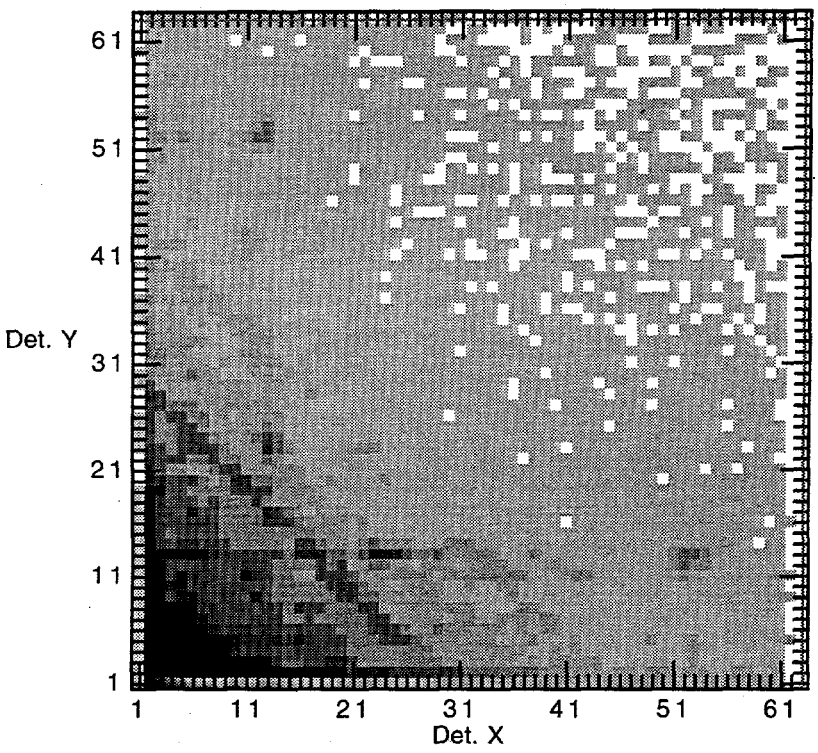


**Figire B.4.** Two-Dimensional Contour Display of Background Coincident Events. Full scale (black) = >200 counts.

# Appendix C

# Data Analysis

# Appendix C

## Data Analysis

The exponential decay of the $^{64}Cu$ activity can be written as:

$$A_t = A_0 \bullet \exp[-\lambda \bullet t] \qquad \text{(Eq. C1.)}$$

where:

$A_t$ = activity at time t
$A_0$ = activity at time $t_0$
$t_0$ = time zero (taken to be the time that the copper was removed from the penetrometer pipe and the neutron source)
$\lambda$ = $\ln 2 / t_{1/2}$
$t_{1/2}$ = half life of $^{64}Cu$ (12.701 hours)

The data acquisition system provides the number of counts ($N_{12}$) observed between times $t_1$ and $t_2$ where:

$t_1$ = the time when counting started
$t_2$ = the time when counting stopped

To obtain $A_0$ (the count rate at $t_0$) we need to know the following time intervals:

$t_{01}$ = the time between the end of irradiation and the start of counting
$t_{12}$ = the elapsed time from the start to finish of the counting period
$t_{12live}$ = the actual time the counting system was taking data which is the elapsed time corrected for counter dead time

The average net count rate ($A_{12}$)over the counting time interval is:

$$A_{12} = (\text{Total counts } (N_{12}) - \text{Bkg. counts} - \text{Compton counts}) / t_{12live} \qquad \text{(Eq. C2.)}$$

Because exponential decay occurs during the counting time interval, the average net count rate must be corrected to the count rate at the beginning of the counting time:

$$A_1 = A_{12} \bullet \lambda \bullet t_{12} / (1 - \exp[-\lambda \bullet t_{12}]) \qquad \text{(Eq. C3.)}$$

To convert $A_1$ to $A_0$, we simply rearrange Eq. C1:

$$A_0 = A_1 / \exp[-\lambda \bullet t_{01}] \qquad \text{(Eq. C4.)}$$

In actual practice, we often obtained several successive counts following a single irradiation. These data were each analyzed by the MITE2 program to obtain $N_{12}$, the background, and the Compton tail. The $A_0$ was calculated for each of these counts separately along with the statistical uncertainty. The individual $A_0$ were combined into a weighted average value. This weighted average value was divided by the saturation factor to obtain the initial activity ($A_{sat}$) corresponding to an infinite irradiation.

$$A_{sat} = A_0 / (1 - \exp[-\lambda \bullet t_{irrad}]) \qquad \text{(Eq. C5.)}$$

where

$t_{irrad}$ = the time interval during which the sample was irradiated with neutrons.

Because the weight of each sample was slightly different, we then divided the saturation activity by the weight of the sample to get the saturation activity per gram of copper ($A_{sat}/g$). This quantity can be plotted versus the moisture content of the barrel in which the sample was irradiated to obtain the calibration curve of count rate versus moisture. This primary calibration curve is very specific for the particular neutron source and the particular counting system used. The uncertainties include only the statistical uncertainties from the counting data, possible errors from the time measurements, and the uncertainties of the water content of the simulated wastes.

It is possible to convert the primary calibration curve to another calibration curve which has more physical significance. The observed saturation activity per gram can be converted to the effective neutron flux at the sample by dividing by several constants:

$$\text{Eff. n flux} = (A_{sat}/g) / (\varepsilon \bullet n \bullet \sigma) \qquad \text{(Eq. C6.)}$$

where:

| | | |
|---|---|---|
| $\varepsilon$ | = $^{64}Cu$ counting efficiency | = 4.29 ± 0.21% |
| n | = number of $^{63}Cu$ atoms per gram of copper | = $6.556 \times 10^{21}$ atoms per g |
| $\sigma$ | = thermal neutron capture cross section for $^{63}Cu$ | = $(4.50 \pm 0.02) \times 10^{-24}$ $cm^2$ per atom |

The effective neutron flux could be compared directly with calculations of the neutron flux based on Monte Carlo codes. Also, the effective neutron flux due to actinides in the actual waste tanks is of more significance than the $^{64}Cu$ count rate caused by that flux. However, a calibration curve based on the effective neutron flux is somewhat less precise than the primary calibration curve because of the uncertainties introduced by the uncertainties on the counting efficiencies (4.9%) and the capture cross section (0.4%).

# Appendix D

## Counting Efficiency for $^{64}Cu$

# Appendix D

## Counting Efficiency for $^{64}Cu$

The absolute calibration of the $^{64}Cu$ counting efficiency in the copper probe geometry required four steps. Step 1 involved the determination of the absolute disintegration rate of a small copper foil using a calibrated germanium diode spectrometer. Step 2 was the conversion of this standard to a liquid form which could be counted on the NaI(Tl) coincidence spectrometer to obtain the efficiency of the liquid geometry. Step 3 was the production and counting of $^{64}Cu$ in the copper probe geometry on the NaI(Tl) coincidence spectrometer. Step 4 was the dissolution of a portion of the copper probe so that it could be counted in the liquid geometry on the NaI(Tl) coincidence spectrometer. The copper probe efficiency was then calculated knowing the weight of the probe mass converted to the liquid geometry and the efficiency for counting in the liquid geometry. More details are given below.

**Step 1**

A small copper disk (0.95-cm diameter and 0.005-cm thick) was irradiated in the neutron multiplier of building 329. This disk was counted in a standard geometry on a germanium diode gamma-ray spectrometer. The disk was first covered top and bottom with 0.0254-cm thick lead foil to assure conversion of the positrons leaving the copper disk. The 0.511-MeV gamma rays produced by the positrons were detected by the germanium spectrometer. The positron branching fraction for $^{64}Cu$ was taken to be $0.193 \pm 0.007$. Because two gamma rays are produced for each annihilation, the effective branching fraction was taken as $0.386 \pm 0.014$. The efficiency for detecting the 0.511-MeV gamma was determined with an uncertainty of 3% by counting a standard traceable to NIST. The $^{64}Cu$ activity was thus determined to be $1.336 \pm 0.063$ μCi as of Sept. 27, 1994 at 8:30 am. The total uncertainty was dominated by the 3% uncertainty from the counting efficiency and the 3.6% uncertainty from the branching fraction.

**Step 2**

The copper disk was dissolved with nitric acid into a 1x6-$in^2$ petri dish along with 9.326 g of non-irradiated high purity copper. The resulting solution was counted in this liquid geometry on the NaI(Tl) coincidence spectrometer. The observed count rate was corrected for radioactive decay to the same time as the standard (8:30 am on Sept. 27, 1994). The counting efficiency for the liquid geometry ($6.967 \pm 0.335\%$) is the corrected count rate divided by the disintegration rate measured for the copper disk. The uncertainty includes the 0.1% uncertainty from counting statistics, the 1% uncertainty from the half-life, the 3% uncertainty from the efficiency calibration of the germanium detector, and the 3.6% uncertainty due to the positron branching fraction for a total uncertainty of 4.81%.

**Step 3**

A standard copper probe (270.38 g) was irradiated by placing the probe in a polyethylene cylinder next to a neutron source. The cylinder was rotated during the irradiation to provide uniform activation of the copper. This probe was then placed in a standard geometry in the NaI(Tl) coincidence spectrometer and counted several times. All the counts were decay corrected to 1:25 pm on Jan. 19, 1995. The average of these counts was 16.650 cpm/g with a statistical uncertainty of 0.3%.

**Step 4**

The copper probe irradiated in Step 3 was wrapped with Teflon tape on the outside and placed in a nitric acid solution. This allowed 11.77 g of copper to be dissolved from the inside of the copper probe. The dissolved copper was counted in the liquid geometry on the NaI(Tl) coincidence spectrometer. Next the copper probe was sealed to prevent acid from reaching the inside and 10.60 g of copper were dissolved from the outside of the probe. This dissolved copper was also counted in the liquid geometry on the NaI(Tl) coincidence spectrometer. Both the inside and outside samples were decay corrected to the same time as in Step 3. Because the absolute efficiency of the liquid geometry had been determined in Step 2, both the inside and outside samples could be converted to absolute disintegrations per minute per gram. The inside sample gave 385.0 dpm/g and the outside sample gave 390.4 dpm/g. The difference between the inside and outside activities was only 1.4% so it was assumed that the copper was uniformly irradiated. The average value of 387.7 ± 19.1 dpm/g was adopted for the disintegration rate. The uncertainty includes all the systematic uncertainties from the calibration of the liquid geometry and the statistical uncertainties from the counting data for a total uncertainty of 4.9%.

The counting efficiency for the copper probe geometry is the cpm/g determined in Step 3 divided by the dpm/g determined in Step 4. This efficiency is 4.29 ± 0.21%.

PNL-10837
UC-606

# Distribution

**No. of Copies**

**Offsite**

2 DOE Office of Scientific and Technical Information

1 Lawrence Livermore National Lab
Attn. J. R Hearst
P.O. Box 808 L221
Livermore, CA 94551

1 RUST Geotech, Inc.
Attn. R.D. Wilson
P.O. Box 14,000
Grand Junction, CO 81502-5504

1 Three Rivers Scientific
Attn. R. R. Randall
3659 Grant Court
W. Richland, WA 99353

**No. of Copies**

**Onsite**

3 *DOE Richland Operations Office*
J.W. Day
R.D. Hildebrand
J.K. Goodenough

1 *NISI*
A.V. Robinson

2 *Westinghouse Hanford Company*
T. M. Hohl
J. E. Meisner
W. T. Watson

27 *Pacific Northwest Laboratory*
M. Bliss
R. L. Brodzinski (5)
R. E. Engelman
W. K. Hensley
R. E. Lewis
P. L. Reeder (5)
D. E. Robertson
D. C. Stromswold (5)
J. M. Tingey (2)
Technical Report Files (5)